



OPEN

Image quality enhancement in variable-refresh-rate AMOLED displays using a variable initial voltage compensation scheme

Li Jin Kim^{1,2}, Sujin Jung¹, Hee Jun Kim¹, Bong Hwan Kim², Kyung Joon Kwon², Yong Min Ha² & Hyun Jae Kim¹✉

In active matrix organic light emitting diode (AMOLED) displays, when a variable refresh rate is applied and the frame rate changes, the image's color and luminance quality in AMOLED displays deteriorates. The frequency-dependent cognitive differences were experimentally demonstrated by using 6.76" AMOLED displays. This phenomenon is dependent on the emission time and the data programming time on the frame rate. This degradation of the image quality during the frequency switch could be prevented by applying a variable initial voltage (V_{ini}) to the OLED anode. For a frequency change between 60 and 120 Hz, the measured just noticeable color difference (JNCD) decreased from 7.50 to less than 1.00 in luminance, and from 2.34 to 0.02 in color. As our approach can prevent image quality distortion by utilizing an existing compensation pixel structure without additional compensation steps, it will be a promising technique for improving the picture quality in AMOLED displays.

Due to the evolutionary trend in the cloud era, and high-speed networks that extend beyond 4th to the 5th generation, interconnections between electronic devices are expanding, and the boundaries between devices such as PCs, TVs, and smartphones are disappearing. In addition, we are approaching to an era in which the enjoyment of contents such as games, movies, and sports require high frame rates, as they retrieve data directly from a cloud server in real time without downloading. Thus, the gradually increasing demand for high refresh rate (HRR, ≥ 90 Hz) driving has gone beyond TVs and PCs to smartphones. However, since HRR driving leads to high power consumption and mobile devices are sensitive to the latter, it is therefore necessary to combine both low refresh rates (LRR) and HRR appropriately to compensate for the high HRR power consumption¹. For example, we can only apply the high-speed driving to moving images such as videos and games, and to scrolling images. To reduce the increasing power consumption raised from HRR driving, a still image is driven by a conventional normal refresh rate (NRR) of 60 Hz, and LRR also could be applied in standby modes such as an always on display (AoD). However, a change in frame rate can deteriorate image quality of active matrix organic light emitting diode (AMOLED) displays, as the threshold voltage compensation¹⁻⁴ and the OLED charging depend on the programming time⁵⁻⁸. In this study, we characterized the image degradation by measuring color and luminance deviations at various frequencies. Furthermore, a new driving method is proposed and it can solve the problem without additional external or internal compensation steps, or modification of the pixel structure.

Experimental section

For the measurements, 6.76" sized 1,344 × 2,772 resolution AMOLED displays with 7T1C compensation pixel structures of low temperature polysilicon (LTPS) thin-film transistors (TFTs) backplane were used. The size of driving TFTs is width/length = 3.0/16.3 μm . KONICA MINORTA's CA-410 was used for optical measurement. The CA-410 was subjected to regular calibration and gage repeatability and reproducibility (R&R) through a standard light source. The measurements were performed at the center of the sample after aging AMOLED displays for 10 min at the maximum luminance to stabilize them. Considering the hysteresis characteristics of TFTs^{9,10}, luminance and color were measured after fixing luminance at each frequency condition, and then this process was repeated for all other luminance conditions. 10 samples were measured in consideration of

¹School of Electrical and Electronic Engineering, Yonsei University, 50 Yonsei-ro, Seodaemun-gu, Seoul 03722, Republic of Korea. ²Mobile Product Development Group, LG Display Co., Ltd, 245 LG-ro, Wollong-myeon, Paju-si, Gyeonggi-do 10845, Republic of Korea. ✉email: hjk3@yonsei.ac.kr

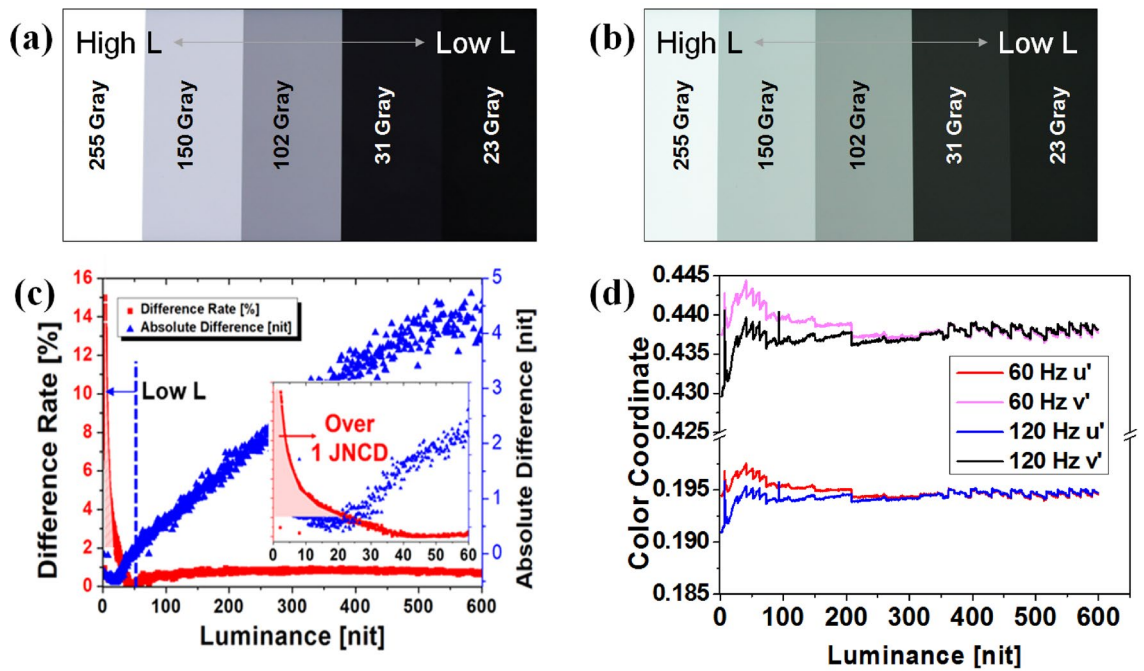


Figure 1. The gamma scale for frequencies of (a) 60 Hz, and (b) 120 Hz, without compensation. The differences in (c) luminance and (d) color, between frequencies of 60 Hz and 120 Hz.

reproducibility and repeatability, and the average value of the measured results was shown as the experimental result. The minimum and maximum luminance of the luminance conditions were 2 and 600 nit respectively. The color space coordinates (u' , v') in the system are defined by the commission internationale de l'Éclairage (CIE) 1976¹¹; the target of color u' and v' are 0.193 and 0.459 respectively. To numerically analyze luminance (L) and color (u' , v') fluctuations, the formulae $\Delta L = (L_2 - L_1/L_2) \times 100$ and $\Delta u'v' = ((u'_1 - u'_2)^2 + (v'_1 - v'_2)^2)^{0.5}$ were used. The just noticeable color difference (JNCD)-a measure for evaluating the color accuracy of a display^{12,13}-was used for comparison. A JNCD value of less than 1 is currently considered excellent. A JNCD value of 1 corresponds to a 0.004 in color ($\Delta u'v'$)^{14,15}. In addition, the result of deriving the luminance deviation corresponding to 0.004 color deviation through the experimental method is at the level of 2%. Furthermore, the JNCD value increases proportionally with the amount of deviation. In this experiment, we defined 60 Hz as NRR and 90 Hz or 120 Hz as HRR. The corresponding 1-frame and 1-horizontal time for each frequency are 16.7 ms/4.5 μ s, 11.1 ms/3.0 μ s, and 8.3 ms/2.1 μ s respectively. The 4.6 V ELVDD and the -3.0 V ELVSS were applied to drive the OLED respectively. The typical V_{INI} was -2.8 V. V_{GH} and V_{GL} were applied with 7.5 V and -8.5 V to drive the gate in panel (GIP) driving, respectively. In addition, our measurement results were cross-confirmed with the simulation using Silvaco's Smart Spice Tool.

Discussion

Figure 1a and b show the gray scale bars displayed by the AMOLED at frequencies of 60 and 120 Hz respectively, with the gray 255 luminance corresponding to 50 nit. Comparing Fig. 1a and b, we confirmed that the color and luminance changed significantly between two corresponding frequency and gray conditions. To analyze the image deterioration numerically, we measured the differences in luminance and colors between 60 and 120 Hz frequency conditions. In Fig. 1c, the right axis shows the absolute difference in luminance, and the left axis shows the difference rate expressed in percentage. Even though the absolute difference is large for high luminance, the difference rate increases as the luminance decreases. As human vision concerning luminance has non-linear characteristics, the cognition of luminance is more sensitive to the difference rate of luminance rather than to the absolute difference¹⁶. Hence, we mainly used the difference rate to describe the results.

In Fig. 1c, it is confirmed that the value of JNCD exceeds 1 under luminance of 20 nit, and increased further as the luminance decreases. We shall explain the root causes of the difference between the two frequency conditions separately in the high and low luminance regions. In the high luminance region, the main cause of luminance deterioration is data leakage, which inevitably occurs in the storage capacitor holding data during 1 frame time. After data programming for the emission, the power of the capacitor is floated, and data leakage occurs over the entire emission period until new data are programmed. Since more leakage occurs during the longer frame time of LRR. Compared to HRR, LRR luminance is lower than HRR luminance in the high-luminance region.

On the other hand, the low-luminance region is driven by a small current, so the OLED saturation characteristics are mainly affected by the parasitic capacitance of the OLED. With HRRs, current flow during OLED charging is disturbed heavily by the parasitic capacitor due to the relatively short emission time compared to LRR. Accordingly, in the low-luminance region, HRR luminance cannot reach the target luminance, thus, HRR luminance is lower than the NRR.

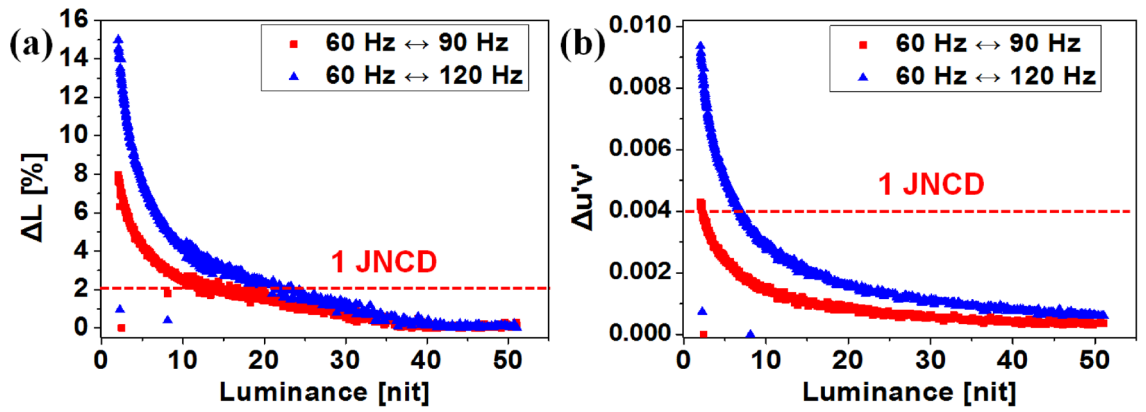


Figure 2. Differences in (a) luminance and (b) color under a frequency change from 60 to 90 Hz and 60 Hz to 120 Hz without V_{INI} compensation.

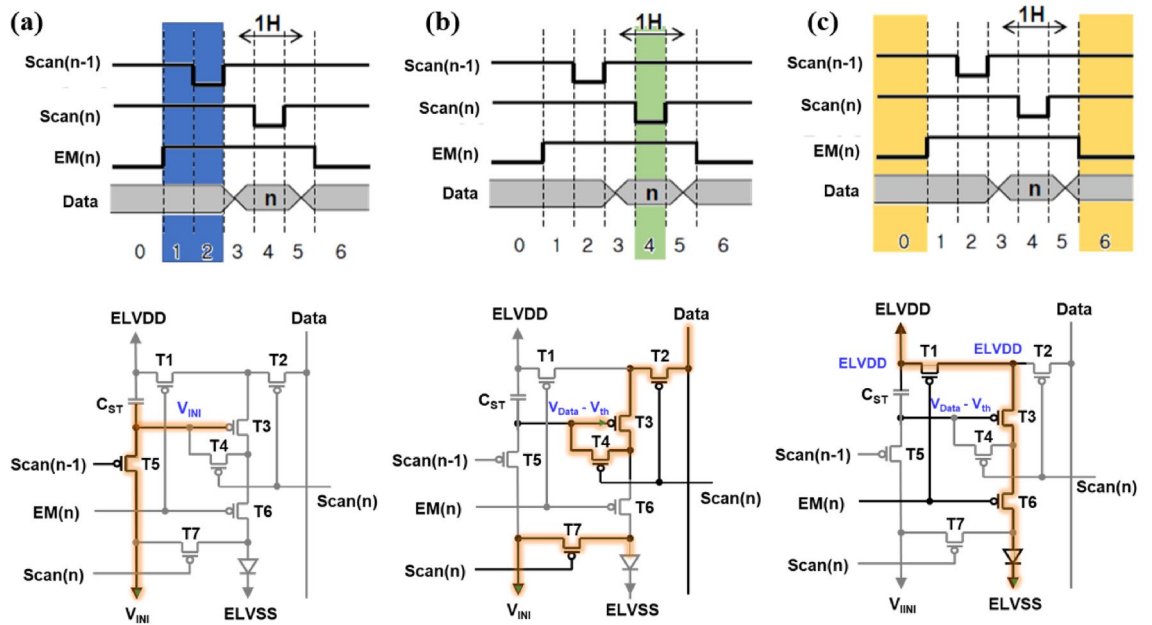


Figure 3. Driving sequence of 7T1C compensation pixels: (a) initialization step, (b) sampling step, (c) emission step.

As shown in Fig. 1c, luminance of less than 50 nits has a negative absolute difference value. This phenomenon is also evident in the color variations in Fig. 1d. In general, the emission efficiencies of red and green OLEDs are higher than that of blue OLEDs. Therefore, in the low-luminance region, the color fluctuates in the direction of increasing values of both u' and v' under HRR, resulting in the color variation shown in Fig. 1b.

Figure 2a and b show the difference in luminance and color after the frequency changes from 60 to 90 Hz, and from 60 to 120 Hz, respectively. We focused on the low luminance region (< 50 nit) where huge differences can be noticed in Fig. 1. The differences in luminance and color between two frequencies increase as a result of the shorter emission and data programming time.

Before explaining the detail mechanism of this phenomenon, the operation sequence of 7T1C compensation structure is described in Fig. 3. First step is (a) initialization, where T_1 and T_6 are turned off by EM signal. T_5 is turned on by Scan[$n - 1$], which means the gate node of driving TFT and storage capacitor are initialized. Next step is (b) sampling. T_2 , T_3 , T_4 , and T_7 are turned on by the Scan[n] signal. Therefore, the threshold voltage (V_{th}) of the driving TFT is stored in the storage capacitor and the OLED anode is initialized. The final step of pixel driving is (c) emission. T_1 , T_3 , and T_6 are turned on by the EM signal, so compensated data voltage is stored in storage capacitor and maintains the emission state. And the formula for the current flowing through the OLED and V_{th} compensation are shown in Eq. (1), where k is the parameter determined by the mobility μ , the oxide capacitance C_{ox} , and channel width (W) and length (L). Therefore the I_{OLED} becomes independent of the V_{th} of driving TFT (T_3).

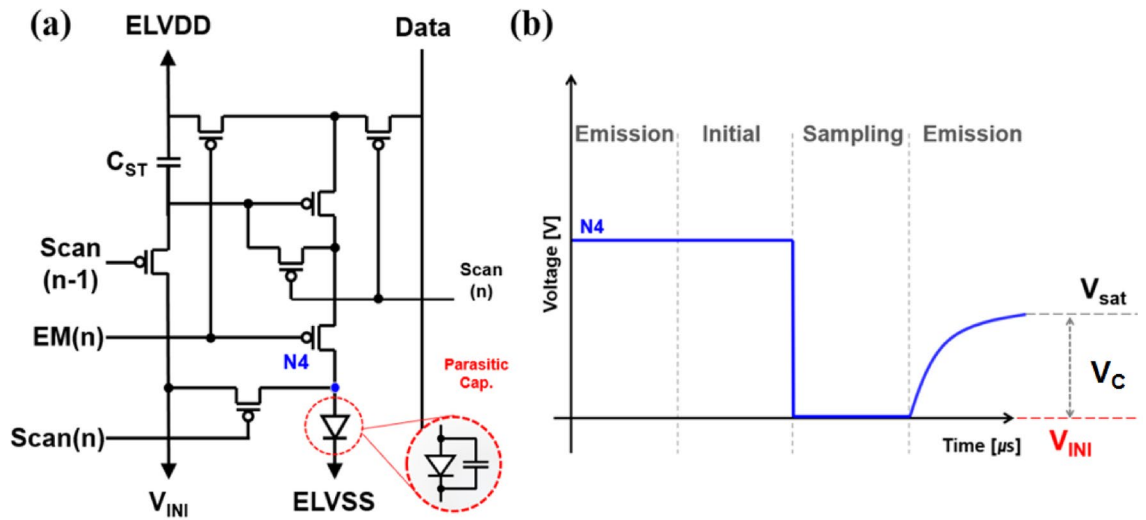


Figure 4. (a) Schematic of a 7T1C pixel circuit. (b) A schematic diagram for the OLED anode node voltage described by the compensation process.

$$\begin{aligned}
 I_{OLED} &= k(V_{GS} - V_{th})^2 = k(ELVDD - V_{Data} + V_{th} - V_{th})^2 \\
 &= k(ELVDD - V_{Data})^2
 \end{aligned}
 \tag{1}$$

Figure 4 shows the mechanism that causes image distortion to occur more often in the low luminance region as the frequency is increased, and how this can be prevented. Figure 4a shows a p-type LTPS 7T1C compensation pixel circuit diagram. During the initialization process, the driving TFT is controlled by the V_{INI} . The V_{INI} resets the gate node and the storage capacitor while simultaneously resetting the anode (N_4) voltage³. The V_{INI} resets the gate node and the storage capacitor and simultaneously resets the anode (N_4) voltage. After the programming step, the N_4 node has the V_{INI} in a floating state. After the programming step, the N_4 node is maintained at the V_{INI} until the emission, and then emitting as the current is applied to the OLED in the emission period. When the OLED is in saturation state, to emit light, it is necessary to apply a voltage to charge the OLED, which can reach the saturation state from the initial state. Since V_{INI} is generally negative, the relationship among the voltage for charging the OLED (V_C), the initial voltage, and the saturation voltage (V_{SAT}) can be expressed as the following:

$$V_C = V_{SAT} - V_{INI}
 \tag{2}$$

The V_{SAT} can be expressed as below formula, which contains the current of specific luminance (I_L), emission time (T_E) and OLED capacitance (C_{OLED}). Then the voltage V_C required for emission can be replaced as the following:

$$V_C = \frac{I_L \times T_E}{C_{OLED}} - V_{INI}
 \tag{3}$$

Due to insufficient current in the low luminance region, charging is not efficient. HRR, given its short sampling and emission time, its charging capacity is weaker than LRR's. It is possible to say that the fluctuation in the anode voltage originates from the starting value of V_{INI} for the anode voltage, as shown in Fig. 4b. At each frequency, to match the charging characteristics to the target V_{SAT} , V_C should be increased by a variable V_{INI} value.

Figure 5 shows the validation for mechanism and improvement through simulation. From the simulation results, it can be seen that when the same V_{INI} was applied under 90 Hz HRR and 60 Hz NRR conditions. The OLED current is significantly reduced in HRR condition due to the charging delay. On the other hand, when the V_{INI} is raised from -2.8 to -2.0 V under the 90 Hz condition, it is confirmed that in 1 frame the current amounts under 90 Hz is similar to 60 Hz. Through the simulation results, it was confirmed that the OLED current deviation during frequency changes could be compensated through V_{INI} control securing the anode voltage charge.

Figure 6 shows the difference rate between 60 and 120 Hz frequency, in different V_{INI} conditions. As the V_{INI} increases, the fractional differences in the quantities become smaller. As can be seen in Fig. 6a and b, depending on the V_{INI} setting, luminance and color difference were improved from 7.5 (15%)/2.25 (0.009) to 5 (10%)/1.5 (0.006) respectively. Image quality distortion will still occur, however, due to the different influence of the parasitic capacitance at each frequency. For further improvement, it will be necessary to adjust the saturation characteristics by applying the V_{INI} individually for each frequency, as mentioned before.

While in Fig. 6, a fixed V_{INI} has been applied for a frequency change between 60 and 120 Hz, we investigated the results when different V_{INI} were used for different frequencies: -2.8 V for 60 Hz, -2.6 V for 90 Hz, and -2.4 V for 120 Hz. The results are shown in Fig. 7a and b. After applying voltage compensations, both color

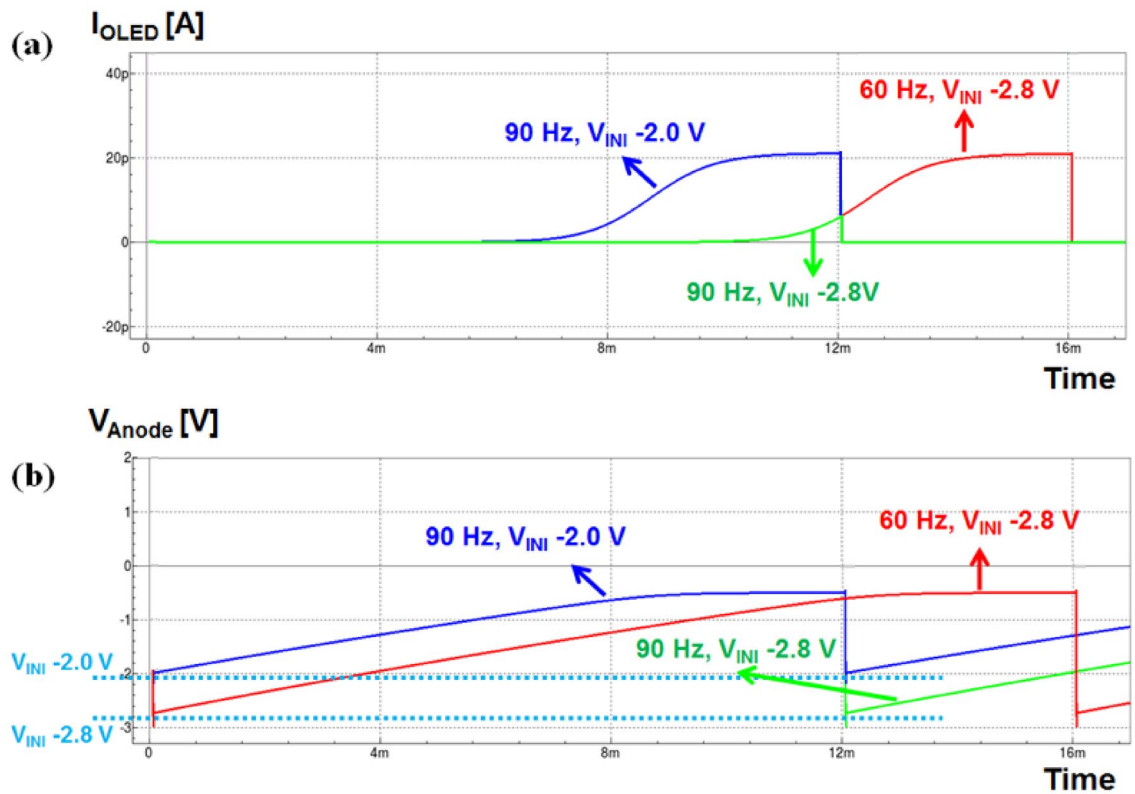


Figure 5. Simulation results for (a) OLED pixel current and (b) anode voltage in various V_{INI} at 60 and 90 Hz conditions.

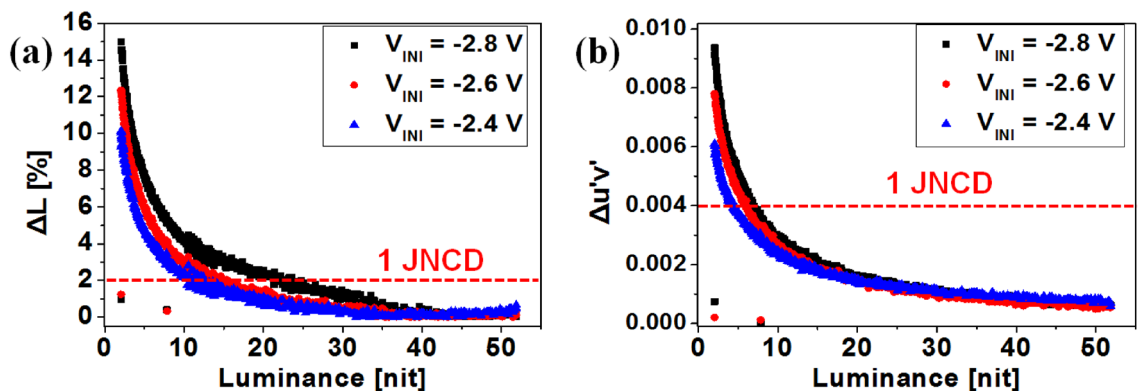


Figure 6. (a) The luminance and (b) color differences for a frequency change from 60 to 120 Hz, with fixed initial voltages of -2.8 , -2.6 , and -2.4 V.

and luminance fluctuations decrease to less than 1 JNCD. In Fig. 7c and d, various gray scales displayed on the 6.76" AMOLED display under different frequency conditions of 60 and 120 Hz, respectively, are shown. After the variable V_{INI} is applied, no corruption in the image quality has occurred even in the case of 120 Hz as well as the case of 60 Hz. Figure 8 shows the box plot data for luminance and color difference before and after the V_{INI} compensation, using 10 samples for each case, to confirm the reproducibility of the proposed method. Reproducibility was verified as can be indicated from the figure where the variations were significantly reduced once the compensation method was applied.

Conclusion

The causes for the degradation in image quality of AMOLED display in variable refresh rate have been examined. At high driving frequencies, we confirm that the effect of parasitic capacitance is significant in the low luminance region. This degradation of image quality in low luminance, which is particularly noticeable to human eyes, can be prevented by applying individual V_{INI} values to the OLED without additional compensation steps. We

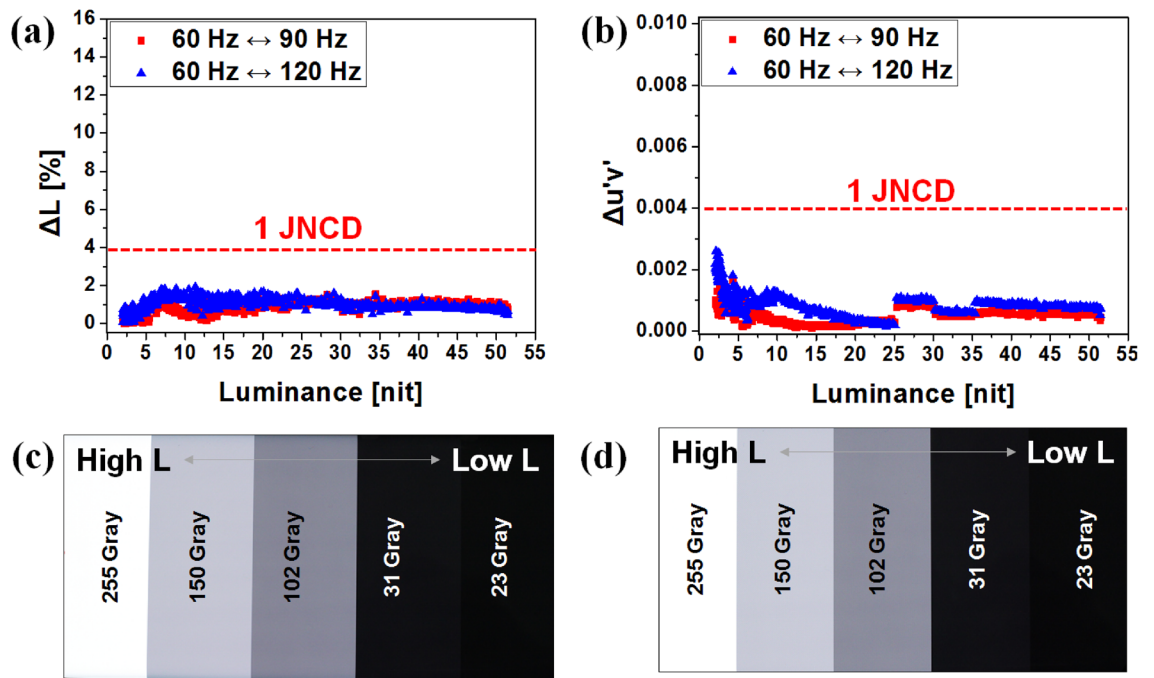


Figure 7. (a) The luminance and (b) color differences under frequency changes. The initial voltages were: -2.8 V for 60 Hz, -2.6 V for 90 Hz, and -2.4 V for 120 Hz. The displayed gamma scales for (c) 60 Hz and (d) 120 Hz, after V_{INI} compensation was applied.

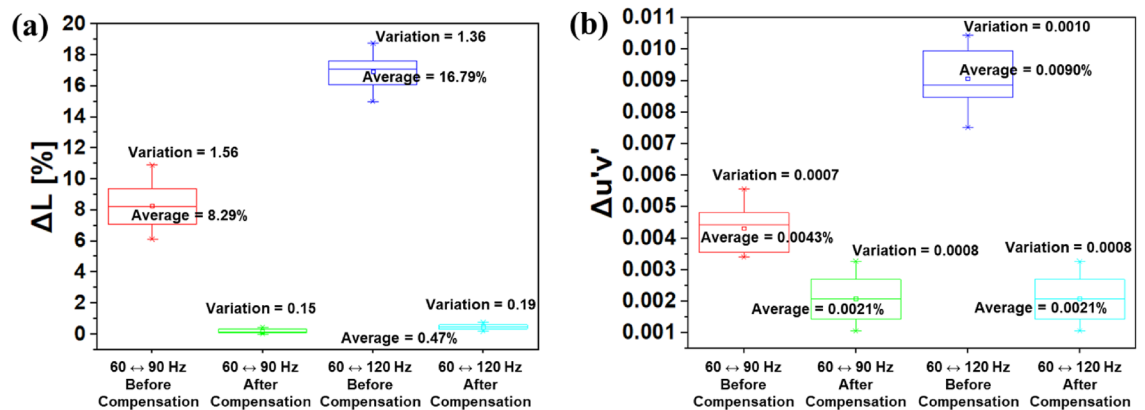


Figure 8. Box plot data for (a) luminance and (b) color differences showing their variation before and after the initial voltage compensation evaluated with 10 samples each.

demonstrated the effectiveness of this technique by applying it to a 6.76" sized AMOLED display panel. When switching frequency from 60 to 120 Hz, the luminance distortion decreased from 7.5 to less than 1 JNCD, and the color quality was improved from 2.34 to 0.02 JNCD, which could not be achieved with the traditional compensation method.

Received: 10 October 2021; Accepted: 15 March 2022
 Published online: 08 April 2022

References

- Kim, J., Chung, H. J. & Lee, S. W. A low-power pixel circuit comprising low-temperature poly-silicon and oxide TFTs for liquid crystal displays with panel self-refresh technology. *IEEE Electron. Dev. Lett.* **41**, 868–871 (2020).
- In, H. J., Jeong, I. H., Kang, J. S., Kwon, O. K. & Chung, H. K. P-8: A novel feedback-type AMOLEDs driving method for large-size panel applications. *SID Symp. Dig. Tech. Pap.* **36**, 252–255 (2005).
- Sohn, Y., Moon, G., Choi, K., Kim, Y. & Park, K. Effects of TFT mobility variation in the threshold voltage compensation circuit of the OLED display. *J. Inf. Disp.* **18**, 25–30 (2017).
- Yoon, M., Park, J., Tran, D. C. & Sung, M. M. Fermi-level engineering of atomic layer-deposited zinc oxide thin films for a vertically stacked inverter. *ACS Appl. Electron. Mater.* **2**, 537–544 (2020).

5. Geffroy, B., Le Roy, P. & Prat, C. Organic light-emitting diode (OLED) technology: Materials, devices and display technologies. *Polym. Int.* **55**, 572–582 (2006).
6. Dawson, R. M. A. *et al.* The impact of the transient response of organic light emitting diodes on the design of active matrix OLED displays. *IEDM Tech. Dig.* 875–878 (1998).
7. Nagar, M. R., Shahnawaz, Y. R. A. K., Lin, J. T. & Jou, J. H. Nanocomposite electron-transport layer incorporated highly efficient OLED. *ACS Appl. Electron. Mater.* **2**, 1545–1553 (2020).
8. Youn, W., Lee, J. W., Yu, H. & Kim, D. Y. Effect of refractive index contrast on out-coupling efficiency of corrugated OLEDs using low-refractive-index LiF interlayer. *ACS Appl. Electron. Mater.* **2**, 2218–2223 (2020).
9. Kim, B. K., Kim, O., Chung, H. J., Chang, J. W. & Ha, Y. M. Recoverable residual image induced by hysteresis of thin film transistors in active matrix organic light emitting diode displays. *Jpn. J. Appl. Phys.* **43**, L482 (2004).
10. Hwang, H. W. *et al.* Analysis of recoverable residual image characteristics of flexible organic light-emitting diode displays using polyimide substrates. *IEEE Electron. Dev. Lett.* **40**, 1108–1111 (2019).
11. Masaoka, K. & Nishida, Y. Metric of color-space coverage for wide-gamut displays. *Opt. Express* **23**, 7802–7808 (2015).
12. Yang, C. H. *et al.* 62-2: Novel thin film encapsulation structure for wearable plastic AMOLED display. *SID Symp. Dig. Tech. Pap.* **47**, 841–843 (2016).
13. Steckel, J. S. *et al.* Quantum dots: The ultimate down-conversion material for LCD displays. *J. Soc. Inf. Disp.* **23**, 294–305 (2015).
14. Ou, Q. D. *et al.* Simultaneously enhancing color spatial uniformity and operational stability with deterministic quasi-periodic nanocone arrays for tandem organic light-emitting diodes. *Adv. Opt. Mater.* **3**, 87–94 (2015).
15. Komoda, T. *et al.* 72.1: Invited paper: High performance white OLEDs for next generation solid state lightings. *SID Symp. Dig. Tech. Pap.* **42**, 1056–1059 (2011).
16. Acharya, T. & Ray, A. K. *Image Processing: Principles and Applications* 37–39 (Wiley, 2005).

Acknowledgements

This work was supported by the LG Display Co., Ltd. and the Nano Material Technology Development Program through the National Research Foundation of Korea (NRF) funded by Ministry of Science and ICT under Grant 2018M3A7B4071521.

Author contributions

L.J.K. organized the data, drew figures, and wrote the main manuscript text. All authors reviewed the results and implications and commented on the manuscript at all stages. The project was guided by H.J.K. (corresponding author).

Competing interests

The authors declare no competing interests.

Additional information

Correspondence and requests for materials should be addressed to H.J.K.

Reprints and permissions information is available at www.nature.com/reprints.

Publisher's note Springer Nature remains neutral with regard to jurisdictional claims in published maps and institutional affiliations.



Open Access This article is licensed under a Creative Commons Attribution 4.0 International License, which permits use, sharing, adaptation, distribution and reproduction in any medium or format, as long as you give appropriate credit to the original author(s) and the source, provide a link to the Creative Commons licence, and indicate if changes were made. The images or other third party material in this article are included in the article's Creative Commons licence, unless indicated otherwise in a credit line to the material. If material is not included in the article's Creative Commons licence and your intended use is not permitted by statutory regulation or exceeds the permitted use, you will need to obtain permission directly from the copyright holder. To view a copy of this licence, visit <http://creativecommons.org/licenses/by/4.0/>.

© The Author(s) 2022